

# Image reconstruction for electrical impedance tomography based on spatial invariant feature maps and convolutional neural network

Delin Hu

School of Engineering  
The University of Edinburgh  
Edinburgh, UK  
delin.hu@ed.ac.uk

Keming Lu

Department of Automation  
Tsinghua University  
Beijing, P.R. China  
lkm16@mails.tsinghua.edu.cn

Yunjie Yang

School of Engineering  
The University of Edinburgh  
Edinburgh, UK  
y.yang@ed.ac.uk

**Abstract**—Data-driven methods are attracting more and more attention in the field of electrical impedance tomography. Many learning-based tomographic algorithms have been presented and investigated in the past few years. However, few related studies pay attention to the symmetrical geometrical structure of tomographic sensors and the possible benefits it may bring to learning-based image reconstruction. Aiming to this, we propose the concept of electrical impedance maps, which can better reflect the nature of geometry of tomographic sensors and have similar properties to images. Then we design a fully convolutional network to build the relationship between electrical impedance maps and conductivity distribution images. The effectiveness and performance of our method is evaluated by both simulation and experimental datasets with different conductivity distribution patterns.

**Index Terms**—electrical impedance tomography, convolutional neural network, data-driven imaging

## I. INTRODUCTION

ELECTRICAL impedance tomography (EIT) is one kind of imaging modality with the properties of non-invasiveness, low cost and easy to deploy, which allows it to be applied in a wide range of scenarios, such as industrial process monitoring [1], [2], cell culture observation [3], etc. The main algorithmic problem in EIT is conductivity distribution reconstruction based on differential voltage measurements through solving an inverse problem [4]. Although numerous methods with regard to this issue have been investigated and published over the past decades, robust and high-resolution conductivity reconstruction is still challenging due to its nonlinearity and ill-posedness.

Recently, as the advancement of deep learning theory and computation power of hardware, an increasing number of researchers attempt to seek new possibilities to address nonlinear ill-posed inverse problem with the assistance of deep learning algorithms [5]. For example, Zheng *et al.* developed an auto-encoder based method to achieve image reconstruction in electrical capacitance tomography (ECT) [6], [7]. Tan *et al.* employed a convolutional neural network (CNN) to establish the relationship between electrical resistance tomography (ERT) measurements and the conductivity distribution

[8]. Kłosowski *et al.* proposed two EIT image reconstruction methods based on fully-connected neural network (FCNN) and CNN respectively [9]. Even though these approaches seem to have better performance on simulation datasets compared with traditional tomographic algorithms, there are still some critical issues that need to be addressed.

First of all, none of these previous studies take the geometrical structure of EIT sensors into account during the design of their network architectures. In fact, the geometry of frequently-used EIT sensors has a high degree of spatial symmetry. This characteristic may help us dramatically reduce the number of parameters of the network without any negative impacts on its performance, and allow the network to leverage feature patterns hiding in measurements more easily, which will further improve the quality of reconstructed images.

Furthermore, for data-driven methods, the generalization ability is one of the most important criteria to evaluate their performance. However, to the best of our knowledge, there are few related studies which pay attention to this issue. Most of the existing data-driven image reconstruction approaches were only tested on samples which have a high degree of similarity with training samples. Verifying the generalization ability of learning-based tomographic algorithms is a prerequisite of practical applications.

In this work, we mainly focus on these two issues, developing a novel deep-learning based image reconstruction method for EIT and evaluate its effectiveness on samples in multiple different testing datasets which are obviously different from training samples. Our contributions are summarized as below:

- We propose the concept of electrical impedance maps (EIMs), which can better reflect the nature of geometry of EIT sensors and therefore benefit image reconstruction compared with differential voltage measurement vectors which are widely used in various learning-based methods at current time.
- We design a fully convolutional network architecture to process EIMs and reconstruct conductivity distribution images. Our presented method is expected to outperform

other existing data-driven methods.

- We carry out simulation and experiments to collect data with different conductivity distribution patterns, and use them to evaluate the effectiveness and performance of the proposed image reconstruction approach.

## II. METHODOLOGY

### A. Electrical impedance maps

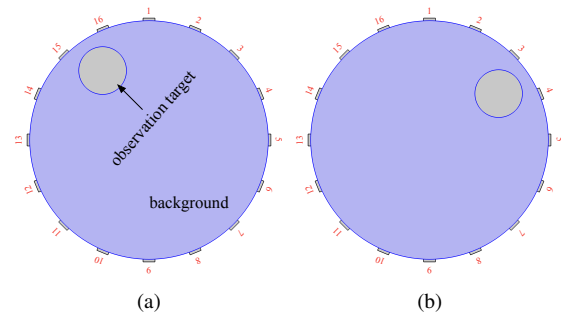


Fig. 1: Examples of a 16-electrode EIT sensor with different inside conductivity distributions. The conductivity is 0.1 S/m for the background material, and is 0.000075 S/m for the observation target. (a) One circle at upper left corner. (b) One circle at upper right corner.

In order to demonstrate the special symmetrical geometry of EIT sensors, we plot Fig. 1. The EIT sensors in Fig. 1 (a) and (b) are exactly the same, and their conductivity distributions are symmetric about the midline between  $e_1$  and  $e_2$  ( $e_i$  represents electrode  $i$  in Fig. 1). The differential voltage measurement between  $e_{15}$  and  $e_{16}$  in (a) should have the same value with the measurement between  $e_3$  and  $e_4$  in (b) when we select  $e_1$  and  $e_2$  as the excitation electrode pair. Similarly, the differential voltage measurements between  $e_1$  and  $e_2$  in both (a) and (b) should be the same when the excitation electrode pairs for (a) and (b) are  $e_{15}, e_{16}$  and  $e_3, e_4$  respectively. Inspired by this characteristic, we can arrange the measurements as a feature map, i.e. the electrical impedance map (EIM).

In this paper, the adjacent measurement strategy is applied, and 208 differential voltage measurements can be eventually obtained. These measurements then are arrayed to form a 16\*16 EIM, which is shown in Fig. 2. The measurement between  $e_j$  and  $e_{j+1}$  when the current supply connects with  $e_i$  and  $e_{i+1}$  is filled in the intersection of the  $i^{th}$  row and the  $j^{th}$  column, and the rest of EIM is padded with 0. Each element in the same row shares the same excitation electrode pair, and each element in the same column shares the same measurement electrode pair.

Fig. 3 shows the EIMs of conductivity distributions in Fig. 1. It is straightforward to observe that the two EIMs have the same feature patterns. The only difference is the locations of these patterns. For instance, the same feature pattern appears at the bottom right corner in the left EIM and the top left corner in the right EIM. This observation and previous analysis about symmetry suggest that the same

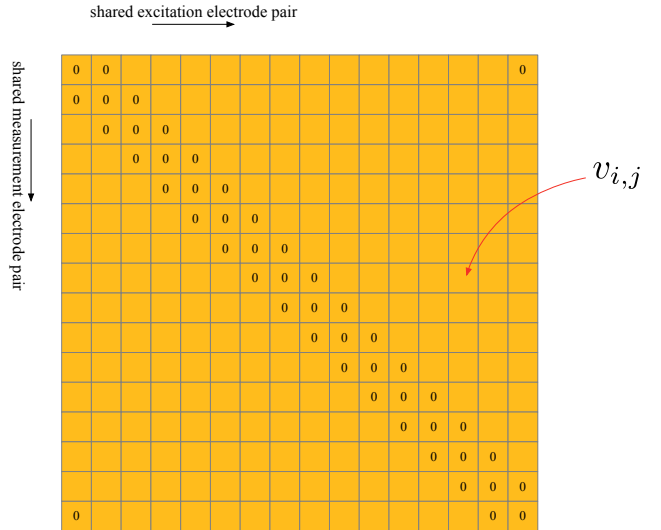


Fig. 2: Electrical impedance maps

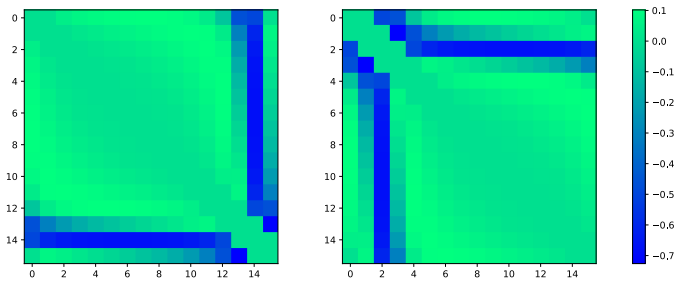


Fig. 3: Examples of EIM. The left one corresponds to Fig. 1 (a), and the right one corresponds to Fig. 1 (b).

pattern appearing at different positions of the EIM may imply that the same objective distributes at different locations in the reconstructed conductivity distribution image. This spatial invariant property is similar to images. We therefore manage to use CNN to process EIMs.

### B. Network architecture

CNN is powerful to analyze data that comes in the form of multiple arrays [10]. Local patch connectivity and weight sharing enable CNN to detect useful feature patterns with a much smaller number of parameters compared with FCNN. This technique has achieved great success in various application scenarios, especially in image processing [11], [12].

The architecture of CNN for processing electrical impedance maps (CNN-EIM) in this paper is shown in Fig. 4. It has 5 convolutional layers and 4 deconvolutional layers. Batch normalization [13] is applied to accelerate training process and prevent overfitting to a certain degree. The filter size, padding and stride for all convolutional layers are 3\*3, 1 and 1 respectively. The same parameters are 2\*2, 0, 2 for the deconvolutional layers and 2\*2, 0, 2 for the max pool layers.

We denote the input (i.e. EIM) as  $v$ , the output (i.e. reconstructed image of conductivity distribution) as  $\hat{x}$ , the ground truth conductivity distribution as  $x$  and the network

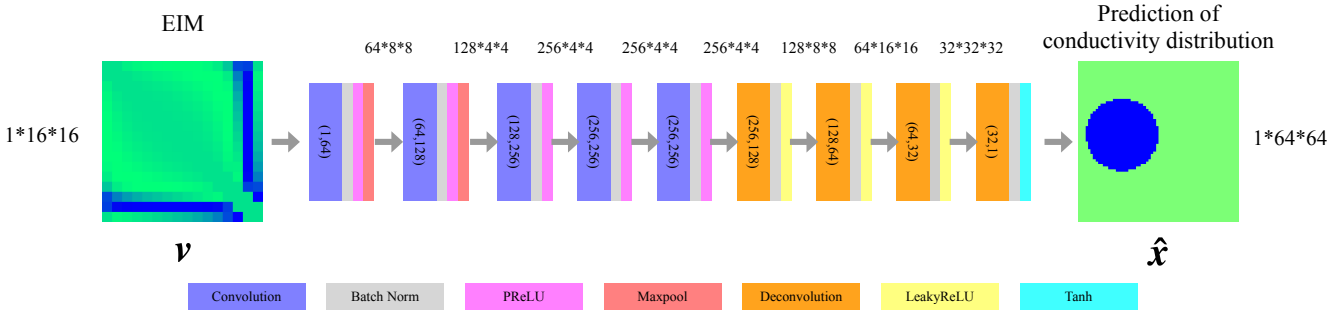


Fig. 4: The framework of CNN-EIM.

CNN-EIM as  $f(\cdot; \theta)$ , where  $\theta$  represents the parameters of CNN-EIM.  $v$  can be mapped to  $\hat{x}$  by  $f(\cdot; \theta)$ , i.e.

$$\hat{x} = f(v; \theta). \quad (1)$$

$\hat{x}$  is expected to be as close as possible to the ground truth conductivity distribution  $x$ . This goal can be achieved by updating the parameters of CNN-EIM  $\theta$  to minimize the loss function  $\mathcal{L}_{recon}(v, x; \theta)$  which is shown as follows:

$$\mathcal{L}_{recon}(v, x; \theta) = \mathbb{E} \|x - f(v; \theta)\|_2^2. \quad (2)$$

However, directly optimizing  $\mathcal{L}_{recon}(v, x; \theta)$  may lead to poor generalization ability and unsMOOTH reconstructed images. We introduce two regularization terms to prevent this issue to some extent, i.e. the total variation regularization term  $\mathcal{L}_{tv}$  [14] and the  $\ell_2$  norm regularization term  $\mathcal{L}_{\ell_2}$ . The complete loss function  $\mathcal{L}(v, x; \theta)$  is

$$\mathcal{L}(v, x; \theta) = \mathcal{L}_{recon} + \lambda_1 \mathcal{L}_{tv} + \lambda_2 \mathcal{L}_{\ell_2} \quad (3)$$

where  $\lambda_1$  and  $\lambda_2$  are hyperparameters for trade-off among different loss terms.

### III. EXPERIMENTS

#### A. Data acquisition

COMSOL and MATLAB joint simulation is used to solve the forward problem of a 16-electrode EIT as shown in Fig. 1 to produce training and testing samples. The inner diameter of the sensing region is 2 m. The conductivity is 0.05 S/m for the background media and 0.0001 S/m for the observation target. The simulation is divided into four different groups according to the number of the observation targets (the number is from 1 to 4). We only consider circular observation targets during simulation, but their diameters and positions are random.

Eventually we totally obtain 29511 samples, including 5261 with 1 circle, 7771 with 2 circles, 7997 with 3 circles and 8482 with 4 circles. Each sample contains a 208-dimensional vector which represents differential voltage measurements and a 3228-dimensional vector which represents the corresponding conductivity distribution and will be transformed to a 64\*64 image.

We established four datasets on the basis of the simulation data, i.e. the training set, validation set, testing set and 3 circles set. The training set contains 15514 samples, while

the validation set and testing set have 3000 samples for each. These three datasets consist of samples with 1, 2 and 4 circles. Samples with 3 circles are grouped into the 3 circles set for further evaluation of the generalization ability of our method, and therefore are not included by the training, validation and testing sets.

We also carry out experiments on our EIT platform [15] to verify the practical effectiveness of our data-driven image reconstruction approach. We collect samples from two different sensors, i.e. the conventional EIT sensor with an internal diameter of 287 mm and the miniature EIT sensor with 16 planar electrodes of which the inner diameter is 15 mm. More details are discussed in section IV. B.

#### B. Implementation details

1) *Calibration and normalization:* The data needs to be calibrated at first, which can reduce the negative impacts of shape and size of sensors. It can be implemented according to Eq. (4)

$$v_{i,j}^c = \frac{v_{i,j} - v_{i,j}^e}{v_{i,j}^e} \quad (4)$$

where  $v_{i,j}^e$  is the  $i^{th}$  row  $j^{th}$  column element in the EIM when the sensing region is filled with the background media,  $v_{i,j}$  is the measurement before calibration and  $v_{i,j}^c$  is the measurement after calibration. In the next step, we apply Eq. (5) to normalize the calibrated data, which can reduce the difficulty in training.

$$v_{i,j}^n = \frac{v_{i,j}^c - \mu_{i,j}}{\sigma_{i,j}} \quad (5)$$

where  $\mu_{i,j}$  and  $\sigma_{i,j}$  represent the mean and the standard deviation of all  $v_{i,j}^c$  in training samples respectively.

2) *Baselines:* In order to better evaluate our approach, we select two learning-based image reconstruction methods as baselines, i.e. CNN for random electrical impedance maps (CNN-REIM) and FCNN for electrical impedance vectors (FCNN-EIV).

The input of CNN-REIM is a REIM which is a 16\*16 matrix and formed by randomly rearranging the elements in the EIM. Note that different EIM generates its corresponding REIM

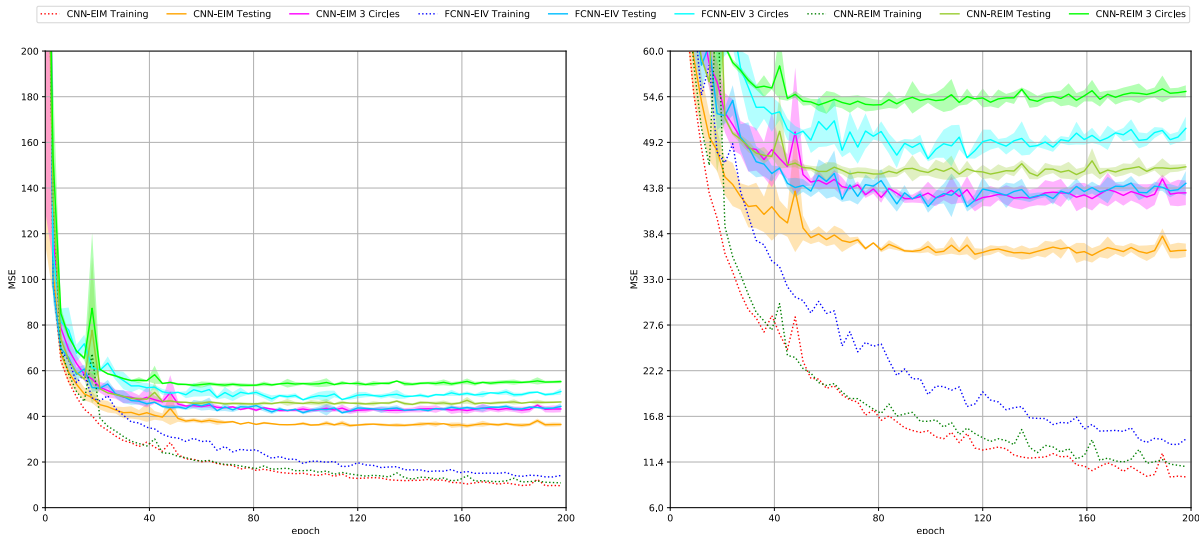


Fig. 5: Training and testing curves for different tomographic methods. The results are the average for 3 runs, and the shadow represents the standard deviation. The right picture is a zoomed-in version of the left one.

based on the same mapping. The structure of CNN-REIM is exactly the same with that of CNN-EIM.

According to *Reciprocity Theorem* [16], a 208-dimensional measurement vector can be compressed to a 104-dimensional measurement vector (i.e. EIV) that acts as the input of FCNN-EIV. The convolutional layers in CNN-EIM are replaced by fully-connected layers in FCNN-EIV which are shown in TABLE I. The deconvolutional parts for both two networks are the same.

TABLE I: FCNN-EIV SPECIFICATION

| Layer | Number of Neurons | $r_p$ |
|-------|-------------------|-------|
| fc1   | 256               | 42    |
| fc2   | 512               | 1.78  |
| fc3   | 1024              | 1.78  |
| fc4   | 2048              | 3.56  |
| fc5   | 4096              | 14.22 |

$r_p$  is the ratio between the number of learnable parameters of the fully-connected layer in FCNN-EIV and the convolution layer in CNN-EIM. Obviously, CNN-EIM has a much smaller number of parameters in comparison with FCNN-EIV.

3) *Training*: Adam [17] is employed to optimize the networks in this work. Learning rate  $\alpha$  is 0.0005. Weights for regularization terms  $\lambda_1$  and  $\lambda_2$  are 500 and 0.00001 respectively. Total number of training epoch is 200. Batch size of each update is 128. Training is implemented on 2 \* Nvidia Quadro P5000. The training time is about 15 mins for CNN and 21 mins for FCNN.

#### IV. RESULTS AND DISCUSSIONS

##### A. Learning curves

The training and testing curves of different methods are illustrated in Fig. 5, where MSE is the mean square error that

equals to  $\mathcal{L}_{recon}$ . We do not plot curves of the validation set in Fig. 5 for clarity as they are very close to the curves of the testing set.

We can observe that CNN-EIM achieves the best performance both in training, testing and 3 circles sets. CNN-EIM converges the fastest during training and has the smallest MSE in testing. From Fig. 5, it also not difficult to find out that CNN-EIM is also less prone to overfitting in comparison with the other two methods. All of these demonstrate the effectiveness of our method.

Moreover, compared with FCNN-EIV, CNN-REIM performs better during training, whilst its testing results on both the testing and 3 circles sets are worse. This suggests that randomly arranging the differential voltage measurements to form feature maps can not bring any benefits for learning-based image reconstruction.

##### B. Image reconstruction

The quality of reconstructed images of CNN-EIM is tested on both simulation samples from the testing and 3 circles datasets and experimental samples from two different EIT sensors.

1) *Simulation results*: Fig. 6 shows the reconstructed images of different algorithms based on simulation data. The sparse Bayesian learning method (SBL) proposed by Liu *et al.* [4] is used for comparison. The samples in the first 5 rows of the figure are from the testing set which have the same image patterns (number of circles) with the training samples but do not appear in training. The last two samples are from the 3 circles set that has a different image pattern from the training set.

It is obvious that image quality of CNN-EIM is the best compared to other methods. Additionally, it can produce satisfactory image reconstruction results for the samples with

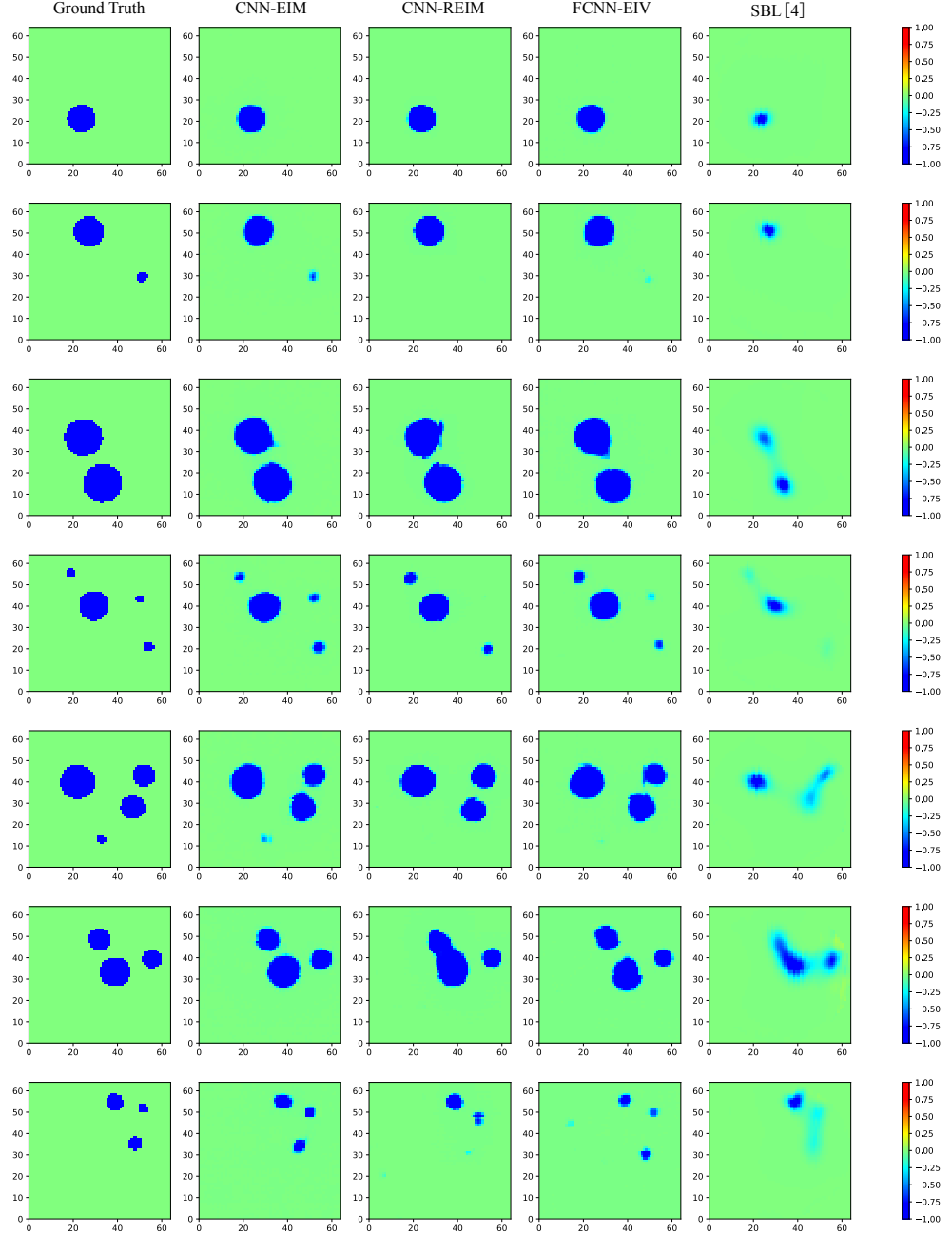


Fig. 6: Image reconstruction results based on simulation data.

3 circles in testing even though it has never seen this type of samples during training. This fact demonstrates the better generalization ability of CNN-EIM in comparison with the other methods.

*2) Experimental results:* Fig. 7 illustrates the reconstructed images of CNN-EIM based on experimental data. For the conventional EIT sensor, the inner diameter is 287 mm. The imaging object is an acrylic rod of which the diameter is around 50 mm, and the background media is saline with the conductivity of around 0.05 S/m. The miniature sensor has

an inner diameter of 15 mm. The imaging object is MCF-7 human breast cancer spheroid of which the diameter is 0.55 mm. The background substance is cell culture media with the conductivity of around 20 S/m.

It is obvious that the setup of the conventional EIT experiment is quite close to its counterpart in simulation. It is not surprising that CNN-EIM is able to provide a satisfactory result under this situation.

Image reconstruction using data produced by the miniature sensor is much more challenging for the learning-based algorithm presented in this paper as there is a significant difference

between the setups of EIT systems generating training and testing samples. However, CNN-EIM can also reconstruct a conductivity distribution image that is quite close to the ground truth distribution as shown in Fig. 7. This further demonstrates the stronger generalization ability of our method.

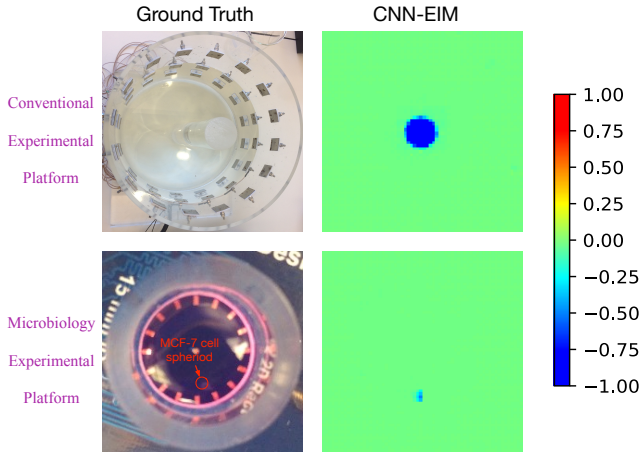


Fig. 7: Image reconstruction results based on experimental data.

## V. CONCLUSIONS

In this paper, we propose the concept of EIMs which are able to better reflect the nature of the symmetrical geometry of EIT sensors and therefore benefit data-driven image reconstruction for EIT. A fully-convolutional neural network (CNN-EIM) is presented to map EIMs to conductivity distribution images. The performance of our method is evaluated by both simulation and experimental datasets. The results show that our approach can achieve higher quality for image reconstruction and better generalization ability with a smaller number of learnable parameters. This demonstrates the effectiveness of EIMs and uncover new possible directions for future research which may link EIMs to other more advanced deep learning algorithms and generate better results.

## REFERENCES

- [1] H. Tapp, A. Peyton, E. Kemsley, and R. Wilson, “Chemical engineering applications of electrical process tomography,” *Sensors and Actuators B: Chemical*, vol. 92, no. 1, pp. 17 – 24, 2003.
- [2] J. Jia, M. Wang, H. I. Schlaberg, and H. Li, “A novel tomographic sensing system for high electrically conductive multiphase flow measurement,” *Flow Measurement and Instrumentation*, vol. 21, no. 3, pp. 184 – 190, 2010.
- [3] Y. Yang, H. Wu, J. Jia, and P. Bagnaninchi, “Scaffold-based 3-d cell culture imaging using a miniature electrical impedance tomography sensor,” *IEEE Sensors Journal*, vol. 19, no. 20, pp. 9071–9080, 2019.
- [4] S. Liu, J. Jia, Y. D. Zhang, and Y. Yang, “Image reconstruction in electrical impedance tomography based on structure-aware sparse bayesian learning,” *IEEE Transactions on Medical Imaging*, vol. 37, no. 9, pp. 2090–2102, 2018.
- [5] T. A. Khan and S. H. Ling, “Review on electrical impedance tomography: Artificial intelligence methods and its applications,” *Algorithms*, vol. 12, no. 5, 2019.
- [6] J. Zheng and L. Peng, “An autoencoder-based image reconstruction for electrical capacitance tomography,” *IEEE Sensors Journal*, vol. 18, no. 3, pp. 5464–5474, 2018.

- [7] J. Zheng, J. Li, Y. Li, and L. Peng, “A benchmark dataset and deep learning-based image reconstruction for electrical capacitance tomography,” *Sensors*, vol. 18, no. 11, 2018.
- [8] C. Tan, S. Lv, F. Dong, and M. Takei, “Image reconstruction based on convolutional neural network for electrical resistance tomography,” *IEEE Sensors Journal*, vol. 19, no. 1, pp. 196–204, 2019.
- [9] G. Kłosowski and T. Rymarczyk, “Using neural networks and deep learning algorithms in electrical impedance tomography,” *Informatics Control Measurement in Economy and Environment Protection*, vol. 7, pp. 99–102, 2017.
- [10] Y. LeCun, Y. Bengio, and G. Hinton, “Deep learning,” *Nature*, vol. 521, pp. 436–444, 2015.
- [11] K. Simonyan and A. Zisserman, “Very deep convolutional networks for large-scale image recognition,” *CoRR, abs/1409.1556v6*, 2014.
- [12] A. Krizhevsky, I. Sutskever, and G. E. Hinton, “Imagenet classification with deep convolutional neural networks,” in *Advances in Neural Information Processing Systems 25*, 2012, pp. 1097–1105.
- [13] S. Ioffe and C. Szegedy, “Batch normalization: Accelerating deep network training by reducing internal covariate shift,” *CoRR, abs/1502.03167v3*, 2015.
- [14] H. Wang, L. Tang, and Z. Cao, “An image reconstruction algorithm based on total variation with adaptive mesh refinement for ect,” *Flow Measurement and Instrumentation*, vol. 18, no. 5, pp. 262 – 267, 2007.
- [15] Y. Yang and J. Jia, “A multi-frequency electrical impedance tomography system for real-time 2d and 3d imaging,” *Review of Scientific Instruments*, vol. 88, no. 8, 2017.
- [16] L. D. Landau, L. P. Pitaevskii, and E. M. Lifshitz, *Electrodynamics of Continuous Media*. Butterworth-Heinemann Ltd, 1984.
- [17] D. P. Kingma and J. L. Ba, “Adam: A method for stochastic optimization,” in *ICLR*, 2015.